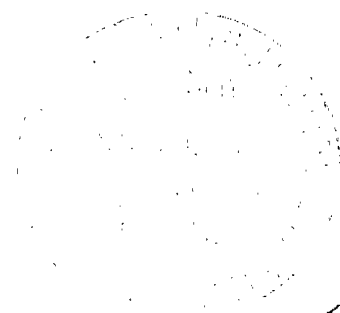**NASA TECHNICAL NOTE**

NASA TN D-7984

$2. u/u$

NUMERICAL CALCULATION OF TRANSONIC BOATTAIL FLOW

Wen L. Chow, Lawrence J. Bober,
and Bernhard H. Anderson

Lewis Research Center
Cleveland, Ohio 44135

NATIONAL AERONAUTICS AND SPACE ADMINISTRATION • WASHINGTON, D. C. • JUNE 1975

1. Report No. NASA TN D- 7984	2. Government Accession No.	3. Recipient's Catalog No.
4. Title and Subtitle NUMERICAL CALCULATION OF TRANSONIC BOATTAIL FLOW		5. Report Date June 1975
		6. Performing Organization Code
7. Author(s) Wen L. Chow, University of Illinois; Urbana, Illinois; Lawrence J. Bober, and Bernhard H. Anderson, Lewis Research Center		8. Performing Organization Report No. E-8065
9. Performing Organization Name and Address Lewis Research Center National Aeronautics and Space Administration Cleveland, Ohio 44135		10. Work Unit No. 505-04
		11. Contract or Grant No.
12. Sponsoring Agency Name and Address National Aeronautics and Space Administration Washington, D.C. 20546		13. Type of Report and Period Covered Technical Note
		14. Sponsoring Agency Code

15. Supplementary Notes

16. Abstract

A viscid-inviscid interaction procedure for the calculation of subsonic and transonic flow over a boattail has been developed. This method couples a finite-difference inviscid analysis with an integral boundary-layer technique. Results indicate that the effect of the boundary layer is as important as an accurate inviscid method for this type of flow. Theoretical results from the solution of the full transonic-potential equation, including boundary layer effects, agree well with the experimental pressure distribution for a boattail. Use of the small disturbance transonic potential equation yielded results that did not agree well with the experimental results even when boundary-layer effects were included in the calculations. The strong interaction characteristics of this type of problem are fully illustrated in this study.

17. Key Words (Suggested by Author(s)) Transonic flow; Boattail pressure distribu- tions; Viscous-inviscid interaction; Finite difference method	18. Distribution Statement Unclassified - unlimited STAR category 02 (rev.)		
19. Security Classif. (of this report) Unclassified	20. Security Classif. (of this page) Unclassified	21. No. of Pages 22	22. Price* $3. 25

NUMERICAL CALCULATION OF TRANSONIC BOATTAIL FLOW

by Wen L. Chow,[*] Lawrence J. Bober, and Bernhard H. Anderson

Lewis Research Center

SUMMARY

A viscid-inviscid interaction procedure for the calculation of subsonic and transonic flow over a boattail has been developed. This method couples a finite-difference inviscid analysis with an integral boundary-layer technique. Results indicate that the effect of the boundary layer is as important as an accurate inviscid method for this type of flow. Theoretical results from the solution of the full transonic-potential equation, including boundary layer effects, agree well with the experimental pressure distribution for a boattail. Use of the small disturbance transonic potential equation yielded results which did not agree well with the experimental results even when boundary layer effects were included in the calculations. The strong interaction characteristics of this type of problem are fully illustrated in this study.

INTRODUCTION

To determine the performance of an air-breathing propulsive system for a supersonic aircraft operating at subsonic cruise conditions, it is necessary that the flow field associated with transonic flow past boattails be successfully analyzed. This type of problem is extremely difficult as the governing inviscid-flow equation is of the mixed type. Furthermore, the relatively short boattail is usually immersed within the thick viscous layer associated with the upstream flow so that the coupling interaction between the viscid and inviscid streams cannot be disregarded. Experimental simulation of such flow conditions has been carried out, for example, by Shrewsbury (ref. 1). Indeed, the experimental data indicated considerable influence of the boattail juncture shape on the pressure distribution on the afterbody, especially at high subsonic free-stream Mach numbers which, in turn, illustrated the extremely sensitive character of the transonic flow.

---

[*]Professor of Mechanical and Industrial Engineering, University of Illinois, Urbana, Illinois.

Since the numerical treatment of external transonic flow using small disturbance theory was made by Murman and Cole (ref. 2), there has been a considerable amount of activity in this area. Krupp and Murman (ref. 3) computed transonic flow past lifting airfoils and slender bodies. Bailey (ref. 4) also extended the small disturbance treatment to calculate transonic flow past slender bodies of revolution. Steger and Lomax (ref. 5) and South and Jameson (ref. 6) used the full potential equation to calculate the transonic flow past two-dimensional and axisymmetric configurations, respectively. However, none of these methods considered the effects of boundary-layer growth on the bodies.

The present study is restricted to the transonic flow field associated with a particular configuration (see fig. 1) used in the experimental program reported in reference 1. Because of the large length to diameter ratio of this configuration, small disturbance theory should be sufficient to calculate the boattail pressure distribution. Such an analysis has indeed produced accurate results for the flow past a parabolic arc of revolution at transonic speeds (ref. 4). These results were reproduced during the present study. This method was applied to the boattail configuration shown in figure 1, and the results are shown in figure 2. The results of the inviscid calculation do not agree well with the data, and the results of the small disturbance theory with boundary layer displacement effects, although in better agreement with the data, do not adequately predict the pressure distribution. This lack of agreement is probably due to the relatively large local curvatures and body slopes present on the body causing large disturbances in the flow field.

It is obvious that the small disturbance treatment is not adequate for this boattail configuration and the full potential equations must be used to study these problems. The results obtained from the present study will illustrate the strong interaction character of these problems within the transonic-flow regime even though flow separation has not been indicated on the boattail.

FUNDAMENTAL EQUATIONS

Inviscid Flow

It has been well established (ref. 7) that, even with the presence of shock waves, the axisymmetric, inviscid, transonic flow field may be described by the potential equation that may be written as (see appendix for definitions of symbols)

$$\left(1 - \frac{\Phi_z^2}{c^2}\right)\Phi_{zz} + \left(1 - \frac{\Phi_r^2}{c^2}\right)\Phi_{rr} - \frac{2\Phi_r\Phi_z}{c^2}\Phi_{rz} + \frac{\Phi_r}{r} = 0 \tag{1}$$

where the subscripts indicate partial differentiation with respect to r and z and where c is the local speed of sound obtained from

$$c^2 = c_0^2 - \frac{\gamma - 1}{2}\left(\Phi_z^2 + \Phi_r^2\right) \tag{2}$$

Upon defining

$$\Phi = V_\infty(z + \varphi) \qquad U = u/V_\infty \qquad V = v/V_\infty \qquad C = c/V_\infty \tag{3}$$

the normalized disturbance potential φ satisfies

$$\left(1 - \frac{U^2}{C^2}\right)\varphi_{zz} + \left(1 - \frac{V^2}{C^2}\right)\varphi_{rr} - \frac{2UV}{C^2}\varphi_{rz} + \frac{\varphi_r}{r} = 0 \tag{4}$$

where

$$U = 1 + \varphi_z$$

$$V = \varphi_r$$

and

$$C^2 = \frac{1}{M_\infty^2} + \frac{\gamma - 1}{2}(1 - U^2 - V^2)$$

$$\left. \right\} \tag{5}$$

Upon introducing the transformation (ref. 6)

$$\xi = z \qquad \zeta = \frac{B\eta}{1 + B\eta} \tag{6}$$

where

$$\eta = r - r_b(z) \tag{7}$$

$r_b(z)$ is the local radius of the body, and B is a stretching parameter, equation (4) becomes

$$\left(1 - \frac{U^2}{C^2}\right)\varphi_{\xi\xi} - B(1 - \zeta)^2\left[2r'_b\left(1 - \frac{U^2}{C^2}\right) + \frac{2UV}{C^2}\right]\varphi_{\xi\zeta}$$

$$+ B^2(1 - \zeta)^4\left[r'^2_b\left(1 - \frac{U^2}{C^2}\right) + \left(1 - \frac{V^2}{C^2}\right) + \frac{2UV}{C^2}r'_b\right]\varphi_{\zeta\zeta}$$

$$+ B(1 - \zeta)^2\left\{\frac{1}{r_b + \dfrac{\zeta}{B(1 - \zeta)}} - r''_b\left(1 - \frac{U^2}{C^2}\right) - 2B(1 - \zeta)\left[r'^2_b\left(1 - \frac{U^2}{C^2}\right) + \left(1 - \frac{V^2}{C^2}\right) + \frac{2UV}{C^2}r'_b\right]\right\}\varphi_{\zeta} = 0 \qquad (8)$$

In the ξ, ζ-coordinate system the normalized velocities are given by

$$U = 1 + \varphi_{\xi} - r'_b\varphi_{\zeta}B(1 - \zeta)^2$$

and

$$V = \varphi_{\zeta}B(1 - \zeta)^2 \qquad (9)$$

where r'_b and r''_b are, respectively, the first and second derivatives of $r_b(z)$. This sheared cylindrical coordinate system is used throughout the flow field since boattail models are usually provided with pointed rather than blunt forebodies. Thus, an orthogonal coordinate system, as used by South and Jameson (ref. 6) for blunt forebodies to insure numerical stability, is not needed. The flow field to be considered in the ξ, ζ-plane is now $-\infty < \xi < +\infty$, $0 \le \zeta \le 1$. It is the experience derived from this study that, with the body situated from zero to one along the axis, the limits of $\xi = -2$ and $\xi = 3$ can be treated as the upstream and downstream limits in the ξ direction. The physical and computational planes are shown in figure 3.

Physically, the flow should be undisturbed at very large distances from the body. Thus, the disturbed potential should vanish at $\xi = -2$, $\xi = 3$, and also at $\zeta = 1$ ($\eta \to \infty$). The boundary condition on the body surface is given by

$$V = r'_b U \quad \text{at} \quad \zeta = 0 \ (\eta = 0) \qquad (10)$$

which may be reduced to

$$\varphi_{\zeta}(\xi, \zeta = 0) = \frac{r'_b}{B\left(1 + r'^2_b\right)}\left[1 + \varphi_{\xi}(\xi, \zeta = 0)\right] \qquad (11)$$

4

For locations along the ξ-axis where $\zeta = 0$ and $r_b = 0$ (upstream of the body and downstream of the body when the model has no sting support) the term φ_r/r in equation (4) is indeterminate since both φ_r and r are zero. In the limit as $r \to 0$ the term $\varphi_r/r \to \varphi_{rr}$ and the terms in equation (8) are correspondingly modified. For convenience, equation (8) is rewritten as

$$EF\varphi_{\zeta\zeta} + H\varphi_{\xi\zeta} + D\varphi_{\xi\xi} + S = 0 \tag{12}$$

where

$$E = B^2(1 - \zeta)^4$$

$$F = r_b'^2\left(1 - \frac{U^2}{C^2}\right) + \left(1 - \frac{V^2}{C^2}\right) + \frac{2UV}{C^2}r_b'$$

$$H = -B(1 - \zeta)^2\left[2r_b'\left(1 - \frac{U^2}{C^2}\right) + \frac{2UV}{C^2}\right]$$

$$D = 1 - \frac{U^2}{C^2}$$

$$\left.\rule{0pt}{120pt}\right\} \tag{13}$$

and

$$S = \varphi_\zeta B(1 - \zeta)^2\left[\cfrac{1}{r_b + \cfrac{\zeta}{B(1 - \zeta)}} - r_b''\left(1 - \frac{U^2}{C^2}\right) - 2B(1 - \zeta)F\right]$$

Equation (12) can be solved by a numerical relaxation scheme. It was pointed out by Murman and Cole (ref. 2) that in solving the transonic flow problem by numerical calculations, different finite-difference formulations should be adopted depending whether the local flow is subsonic or supersonic. For the present problem variable grid size is used in formulating the finite differences in the ξ-direction, and uniform size is adopted in the ζ-direction. For the grid point situated at ξ_j and ζ_k, the equivalent finite difference forms of φ_ξ, $\varphi_{\xi\xi}$, $\varphi_{\xi\zeta}$, φ_ζ, and $\varphi_{\zeta\zeta}$ may be written as

$$\varphi_\xi = \frac{\Delta\xi_1}{\Delta\xi_2(\Delta\xi_1 + \Delta\xi_2)}\,\varphi_{j+1}^k + \frac{\Delta\xi_2 - \Delta\xi_1}{\Delta\xi_1\,\Delta\xi_2}\,\varphi_j^k - \frac{\Delta\xi_2}{\Delta\xi_1(\Delta\xi_1 + \Delta\xi_2)}\,\varphi_{j-1}^k$$

$$= AB1\cdot\varphi_{j+1}^k + AB2\cdot\varphi_j^k + AB3\cdot\varphi_{j-1}^k$$

$$\varphi_{\xi\xi} = \frac{2}{\Delta\xi_2(\Delta\xi_1 + \Delta\xi_2)}\,\varphi_{j+1}^k - \frac{2}{\Delta\xi_1\,\Delta\xi_2}\,\varphi_j^k + \frac{2}{\Delta\xi_1(\Delta\xi_1 + \Delta\xi_2)}\,\varphi_{j-1}^k$$

$$= BB1\cdot\varphi_{j+1}^k + BB2\cdot\varphi_j^k + BB3\cdot\varphi_{j-1}^k$$

$$\varphi_{\xi\zeta} = \frac{1}{2\,\Delta\zeta}\left[AB1\cdot\left(\varphi_{j+1}^{k+1} - \varphi_{j+1}^{k-1}\right) + AB2\cdot\left(\varphi_j^{k+1} - \varphi_j^{k-1}\right) + AB3\cdot\left(\varphi_{j-1}^{k+1} - \varphi_{j-1}^{k-1}\right)\right]$$

$$(14)$$

for locally subsonic flow,

$$\varphi_\xi = \frac{\Delta\xi_0 + 2\,\Delta\xi_1}{\Delta\xi_1(\Delta\xi_0 + \Delta\xi_1)}\,\varphi_j^k - \frac{\Delta\xi_1 + \Delta\xi_0}{\Delta\xi_1\,\Delta\xi_0}\,\varphi_{j-1}^k + \frac{\Delta\xi_1}{\Delta\xi_0(\Delta\xi_0 + \Delta\xi_1)}\,\varphi_{j-2}^k$$

$$= AP1\cdot\varphi_j^k + AP2\cdot\varphi_{j-1}^k + AP3\cdot\varphi_{j-2}^k$$

$$\varphi_{\xi\xi} = \frac{2}{\Delta\xi_1(\Delta\xi_1 + \Delta\xi_0)}\,\varphi_j^k - \frac{2}{\Delta\xi_0\,\Delta\xi_1}\,\varphi_{j-1}^k + \frac{2}{\Delta\xi_0(\Delta\xi_1 + \Delta\xi_0)}\,\varphi_{j-2}^k$$

$$= BP1\cdot\varphi_j^k + BP2\cdot\varphi_{j-1}^k + BP3\cdot\varphi_{j-2}^k$$

$$\varphi_{\xi\zeta} = \frac{1}{2\,\Delta\zeta}\left[AP1\cdot\left(\varphi_j^{k+1} - \varphi_j^{k-1}\right) + AP2\cdot\left(\varphi_{j-1}^{k+1} - \varphi_{j-1}^{k-1}\right) + AP3\cdot\left(\varphi_{j-2}^{k+1} - \varphi_{j-2}^{k-1}\right)\right]$$

$$(15)$$

for locally supersonic flow, and

$$\varphi_\zeta = \frac{\varphi_j^{k+1} - \varphi_j^{k-1}}{2\,\Delta\zeta}$$

$$\varphi_{\zeta\zeta} = \frac{\varphi_j^{k+1} - 2\varphi_j^k + \varphi_j^{k-1}}{(\Delta\zeta)^2}$$

$$(16)$$

6

where

$$\Delta \xi_2 = \xi_{j+1} - \xi_j$$

$$\Delta \xi_1 = \xi_j - \xi_{j-1} \tag{17}$$

$$\Delta \xi_0 = \xi_{j-1} - \xi_{j-2}$$

Equation (12) can be written in finite-difference form for the point (ξ_j, ζ_k) and is given by

$$\left(E \cdot F + \frac{H \Delta \zeta}{2} \cdot AB2 \right) \varphi_j^{k+1} + (-2E \cdot F + \Delta \zeta^2 D \cdot BB2) \varphi_j^k + \left(E \cdot F - \frac{H \Delta \zeta}{2} \cdot AB2 \right) \varphi_j^{k-1}$$

$$= -\frac{H \Delta \zeta}{2} \left[AB1 \cdot \left(\varphi_{j+1}^{k+1} - \varphi_{j+1}^{k-1} \right) + AB3 \cdot \left(\varphi_{j-1}^{k+1} - \varphi_{j-1}^{k-1} \right) \right]$$

$$- \Delta \zeta^2 \left[D \cdot \left(BB1 \cdot \varphi_{j+1}^k + BB3 \cdot \varphi_{j-1}^k \right) + S \right] \tag{18}$$

for subsonic flow, and

$$\left(E \cdot F + \frac{H \Delta \zeta}{2} AP1 \right) \varphi_j^{k+1} + (-2E \cdot F + \Delta \zeta^2 D \cdot BP1) \varphi_j^k + \left(E \cdot F - \frac{H \Delta \zeta}{2} \cdot AP1 \right) \varphi_j^{k-1}$$

$$= -\frac{H \Delta \zeta}{2} \cdot \left[AP2 \cdot \left(\varphi_{j-1}^{k+1} - \varphi_{j-1}^{k-1} \right) + AP3 \cdot \left(\varphi_{j-2}^{k+1} - \varphi_{j-2}^{k-1} \right) \right]$$

$$- \Delta \zeta^2 \left[D \cdot \left(BP2 \cdot \varphi_{j-1}^k + BP3 \cdot \varphi_{j-2}^k \right) + S \right] \tag{19}$$

for supersonic flow. The boundary condition (eq. (11)) is introduced for all points on the ξ-axis ($\zeta = 0$, $k = 1$ for all grid points on the ξ-axis) by introducing a row of grid points at $\zeta = -\Delta \zeta$ whose values of φ $\left(\text{identified as } \varphi_j^b\right)$ are given by

$$\varphi_j^b = \varphi_j^{k=2} - 2 \Delta \zeta \varphi_\zeta (\xi_j, \zeta = 0) \tag{20}$$

where $\varphi_\zeta(\xi_j, \zeta = 0)$ is computed from equation (11) with φ_ξ again evaluated depending whether the flow there is supersonic or subsonic.

7

Since the line relaxation process will be used for the numerical calculations, equation (18) or (19) may be written for all grid points in the same column with the result that the coefficient matrix for the system of equations of φ is tridiagonal. These equations may be easily solved by standard and efficient methods. The information at a grid point used to account for the boundary condition ($\zeta = -\Delta\zeta$) is updated immediately after the calculations for this column are completed.

Viscous Flow

It was noted previously that the viscous layer will be expected to modify and influence significantly the inviscid flow field; an accurate description of the growth of the turbulent boundary layer is thus necessary. Although more sophisticated methods of prediction of its growth are available (refs. 8 and 9), a simple calculation of the growth of the turbulent boundary layer by the integral method of Sasman and Cresci (ref. 10) and then modifying the body into an equivalent inviscid geometry by adding the displacement thickness to the original body are sufficient to account for viscous effects in the flow. Essentially, a pair of ordinary differential equations describing the growth of the momentum thickness θ_c and the form factor H_c of the boundary layer may be written as (ref. 10)

$$\frac{df}{dx} = 1.268\left[\frac{-f}{M_e}\frac{dM_e}{dx}(1 + g_wH_i) - \frac{f}{r_b}\frac{dr_b}{dx} + A\right] \tag{21}$$

and

$$\frac{dH_i}{dx} = -\frac{1}{2M_e}\frac{dM_e}{dx}\left[H_i(H_i + 1)^2(H_i - 1)\right]\left[1 + (g_w - 1)\frac{H_i^2 + 4H_i - 1}{(H_i + 1)(H_i + 3)}\right]$$

$$+ \frac{H_i^2 - 1}{f}A\left[H_i - \frac{0.011(H_i + 1)(H_i - 1)^2}{H_i^2}\frac{2}{c_f}\frac{T_{0,e}}{\overline{T}}\right] \tag{22}$$

where

$$f = \left(\frac{M_e c_0 \theta_i}{\nu_0}\right)^{1.268}$$

$$\theta_i = \theta \left(\frac{T_e}{T_{0,e}}\right)^{(\gamma+1)/[2(\gamma-1)]}$$

$$g_w \equiv \frac{T_w}{T_{0,e}}$$

$$A = 0.123\, e^{-1.561\, H_i} \left(\frac{M_e c_0}{\nu_0}\right)\left(\frac{T_e}{\overline{T}}\right)\left(\frac{T_e}{T_{0,e}}\right)^3 \left(\frac{\mu}{\mu_0}\right)^{0.268}$$

$$\frac{\overline{T}}{T_{0,e}} = 0.5 \frac{T_w}{T_{0,e}} + 0.22\, Pr^{1/3} + (0.5 - 0.22\, Pr^{1/3}) \frac{T_e}{T_{0,e}}$$

$$H_c = H_i g_w \left(1 + \frac{\gamma-1}{2} M_e^2\right) + \frac{\gamma-1}{2} M_e^2$$

$$\frac{c_f}{2} = 0.123\, e^{-1.561\, H_i} \left(\frac{M_e c_0 \theta_i}{\nu_0}\right)^{-0.268} \left(\frac{T_e}{\overline{T}}\right)\left(\frac{\mu}{\mu_0}\right)^{0.268}$$

(23)

and x is the length along the surface of the body.

Since the inviscid flow is established through the relaxative numerical calculations by repeatedly sweeping from upstream toward downstream in the flow field, it is expedient to account for the viscous flow effects by performing the boundary-layer calculations at the end of each sweep (iteration) of the inviscid flow field with the prevailing inviscid flow results on the equivalent body surface as the guiding free-stream information. A new body geometry is obtained through the displacement thickness correction procedure and is used for the next sweep of the inviscid flow field. The final flow pattern is established when the successive change of the disturbed potential is less than an arbitrarily small number (e.g., 3.0×10^{-6}) for all grid points throughout the field.

9

METHOD OF CALCULATION

The flow field in the ξ, ζ-plane ($0 \le \zeta \le 1$, $-2 \le \xi \le 3$) is discretized into a system of finite points. There are 26 points in each column, which are uniformly spaced in the ζ-direction. The suggestion of successive refinement of grid spacing by South and Jameson (ref. 6) is used for grid points along the ξ-direction; thus, the number of grid points in each row changes from 26 to 51 and finally to 101. This distribution of points was used for all results shown in this report. The stretching parameter B (eq. (6)) was set to 8 for all results obtained from this series of calculations. Different values of B did not materially affect the results. Also, below a free-stream Mach number of 0.9, there is no trouble in the convergence of the inviscid calculations toward the final solutions, and over-relaxation factors as high as 1.5 were used to reduce the computational time. For the free-stream Mach number of 0.9, some under-relaxation was required. However, because of the extremely sensitive character of the transonic flow, damping is required for the successive change in the equivalent inviscid body configuration when viscous flow equations are incorporated into calculations. This damping is more important at higher subsonic free-stream Mach numbers. A damping ratio of 2:1 defines

$$\delta^*_{cor, i+1} = \frac{2 \cdot \delta^*_{cor, i} + \delta^*_i}{3} \tag{24}$$

where $\delta^*_{cor, i+1}$ is the δ^* to be applied for the correction to the body geometry for the forthcoming $(i + 1)^{th}$ inviscid calculation, $\delta^*_{cor, i}$ is the δ^* added to the body geometry for the ith inviscid calculation, and δ^*_i is the δ^* calculated from the boundary-layer calculation on the ith iteration. To illustrate the sensitivity of the results, the damping and its effect, the intermediate variation of C_p values at the final point on the boat-tail ($\xi = 1$) is shown in figure 4. The results obtained with a damping ratio of 2:1 are shown in figure 4(a) for the fine mesh size. The pressure coefficient at the end of the boattail is diverging (rather than converging), and, on the 45th iteration with the fine grid, program execution was terminated. When no damping was used in the calculations, termination occurred on the fourth iteration. No severe oscillations were observed in the coarse or medium mesh calculations, and convergence was relatively rapid whether or not damping was used. When the damping ratio was increased to 3:1 (fig. 4(b)), a slowly converging pattern was observed. Rapid convergence was obtained with a damping ratio of 3:1 when boundary-layer calculations and displacement-thickness corrections to the actual body shape were made at every other iteration as shown in figure 4(a)).

All viscous-flow calculations were based on the nominal flow conditions under which the model was tested. These conditions are given in the following table:

Free-stream Mach number, M_∞	Stagnation point pressure, p_0, N/m^2	Stagnation point temperature, T_0, K	Reynolds number per meter, Re/m
0.56	1.24×10^5	329	1.18×10^7
.70	1.19	$\downarrow$	1.32
.80	1.17		1.39
.90	1.15		1.45

RESULTS OF CALCULATIONS

The inviscid-flow results can be obtained by bypassing the viscous-flow calculations. The inviscid results for the four Mach numbers investigated are shown in figure 5, as are the results obtained when the viscous effects are taken into account. A substantial modification of the inviscid results due to the viscous-flow effects has occurred. In addition, the final results agree well with the experimental data, and the strong interaction character of the transonic flow past boattails is thus fully illustrated. For $M_\infty = 0.9$ a slightly higher pressure level in the last part of the boattail surface and an overshoot of shock recompression can be observed.

The corresponding boundary-layer flow properties are presented in figures 6 to 8. Faster rates of increase of δ^*, θ, H_i, and H_c on the last part of the boattail surface are expected because of the adverse pressure gradient in this region. If $H_i \geq 2.0$ is taken to indicate flow separation, the results (fig. 8(a)) indicate that the flow has not separated from the boattail.

To obtain these results (including viscous effects), the approximate amounts of computational time required (with $\epsilon = 3 \times 10^{-6}$) for various free-stream Mach numbers M_∞ are

Free-stream Mach number, M_∞	Computer (CDC 6600 CPU) time, min
0.56	1.9
.7	2.0
.8	2.1
.9	3.2

It has been observed that, when ϵ is changed to 1×10^{-6}, the results are not significantly different and it is not worthwhile to use computational time. On the other hand, when ϵ is changed to 1×10^{-5}, convergence may be indicated even when the oscillatory pattern has not been completely eliminated.

CONCLUSIONS

When viscous flow equations are incorporated into the calculations, damping the changes in the displacement thickness between iterations is definitely needed, particularly for cases with high subsonic free-stream Mach numbers. This is by no means in conflict with the conventional belief that the viscous flows are relatively insensitive to varying external flow conditions. It is the extremely sensitive character of the inviscid transonic flow that makes damping the change in the equivalent inviscid geometry necessary. In fact, for higher subsonic free-stream Mach numbers ($M_\infty \rightarrow 1$), underrelaxation of the potential is needed (ref. 6) even for purely inviscid flow calculations (fixed body geometry).

At free-stream Mach 0.8 and below, the theoretical boattail static-pressure distributions were in reasonable agreement with data, although the theoretical results indicated slightly higher pressures near the end of the boattail. At $M_\infty = 0.9$ this discrepancy is considerably larger. Whether the viscous flow analysis needs more refinement (such as normal pressure difference across the viscous layer or shock-wave - boundary-layer interaction) or the flow has been intermittently separated on this portion of the surface is yet to be examined.

Lewis Research Center,
National Aeronautics and Space Administration,
Cleveland, Ohio, February 28, 1975,
505-04.

APPENDIX - SYMBOLS

A   function for boundary-layer calculations, defined in eqs. (23)

AB1, AB2, AB3   coefficient functions at point where flow is subsonic, defined in
                          eqs. (14)

AP1, AP2, AP3   coefficient functions at point where flow is supersonic, defined in
                          eqs. (15)

B   radial stretch parameter

BB1, BB2, BB3   coefficient functions at point where flow is subsonic, defined in
                          eqs. (14)

BP1, BP2, BP3   coefficient functions at point where flow is supersonic, defined in
                          eqs. (15)

C   dimensionless speed of sound

C_p pressure coefficient, $(p - p_\infty)/\frac{1}{2}\rho_\infty V_\infty^2$

C_p^* pressure coefficient corresponding to local sonic flow

c   local speed of sound

c_f skin friction coefficient

D   coefficient in inviscid analysis, defined in eqs. (13)

D_{max} maximum model diameter

D_s sting diameter

E   coefficient in inviscid analysis, defined in eqs. (13)

F   coefficient in inviscid analysis, defined in eqs. (13)

H   coefficient in inviscid analysis, defined in eqs. (13)

H_c shape factor of compressible boundary layer

H_i shape factor of incompressible boundary layer

L   body length to end of boattail

M   Mach number

Pr   Prandtl number

p   pressure

R   boattail juncture radius of curvature

Re/m   Reynolds number per meter, $\rho_\infty V_\infty/\mu_\infty$

r	radial distance
$r_b(z)$	local body radius
T	temperature
$\overline{T}$	reference temperature for the boundary-layer calculation
U	dimensionless velocity component in axial direction, u/V_∞
u	velocity component in axial direction
V	dimensionless velocity component in radial direction, v/V_∞
V_∞	free stream velocity
v	velocity component in radial direction
x	distance along body surface
z	axial distance from upstream end of model
γ	ratio of specific heats
δ^*	displacement thickness of the boundary layer
δ^*_{cor}	correction to the body to account for viscous effects
$\Delta\zeta$	uniform spacing of the finite grid system in ζ-direction
$\Delta\xi$	nonuniform spacing of the finite grid system in ξ-direction
ζ	transformed radial coordinate
η	transformed coordinate, $r - r_b$
θ_c, θ_i	momentum thickness of the compressible and the corresponding incompressible boundary layers
μ	viscosity
$\overline{\mu}$	viscosity evaluated at $\overline{T}$ temperature
ν	kinematic viscosity
ξ	transformed axial coordinate
Φ	potential function
φ	normalized disturbance potential function

Subscripts:

e	edge of boundary layer
r	partial derivative with respect to r
w	wall

14

z   partial derivative with respect to z

ζ partial derivative with respect to ζ

ξ partial derivative with respect to ξ

0   stagnation state

∞ approaching free stream

REFERENCES

1. Shrewsbury, G. D.: Effect of Boattail Juncture Shape on Pressure Drag Coefficient of Isolated Afterbodies. NASA TM X-1517, 1968.

2. Murman, E. M.; and Cole, J. D.: Calculation of Plane Steady Transonic Flows. AIAA Journal, vol. 9, no. 1, Jan. 1971, pp. 114-121.

3. Krupp, J. A.; and Murman, E. M.: Computation of Transonic Flows Past Lifting Airfoils and Slender Bodies. AIAA Journal, vol. 10, no. 7, July 1972, pp. 880-886.

4. Bailey, F. R.: Numerical Calculation of Transonic Flow About Slender Bodies of Revolution. NASA TN D-6582, 1971.

5. Steger, J. L.; and Lomax, H.: Numerical Calculation of Transonic Flow About Two-Dimensional Airfoils by Relaxation Procedures. AIAA Journal, vol. 10, no. 1, Jan. 1972, pp. 49-54.

6. South, J. C., Jr.; and Jameson, A.: Relaxation Solutions for Inviscid Axisymmetric Transonic Flow Over Blunt or Pointed Bodies. In Computational Fluid Dynamics Conference Proceedings, Palm Springs, Calif., July 19-20, 1973, pp. 8-17.

7. Cole, J. D.; and Messiter, A. S.: Expansion Procedures and Similarity Laws for Transonic Flow. Zeit. Fur Anglwandte Math. und Physik, vol. 8, no. 1, Jan. 1957, pp. 1-25.

8. Kline, S.; Morkovin, M.; Sovran, G.; and Cockrell, D., eds.: Proceedings Computation of Turbulent Boundary Layers. Standford University Press, 1968.

9. Bertram, M. H., ed.: Compressible Turbulent Boundary Layers. NASA SP-216, 1969.

10. Sasman, P. K.; and Cresci, R. J.: Compressible Turbulent Boundary Layer with Pressure Gradient and Heat Transfer. AIAA Journal, vol. 4, no. 1, Jan. 1966, pp. 19-25.
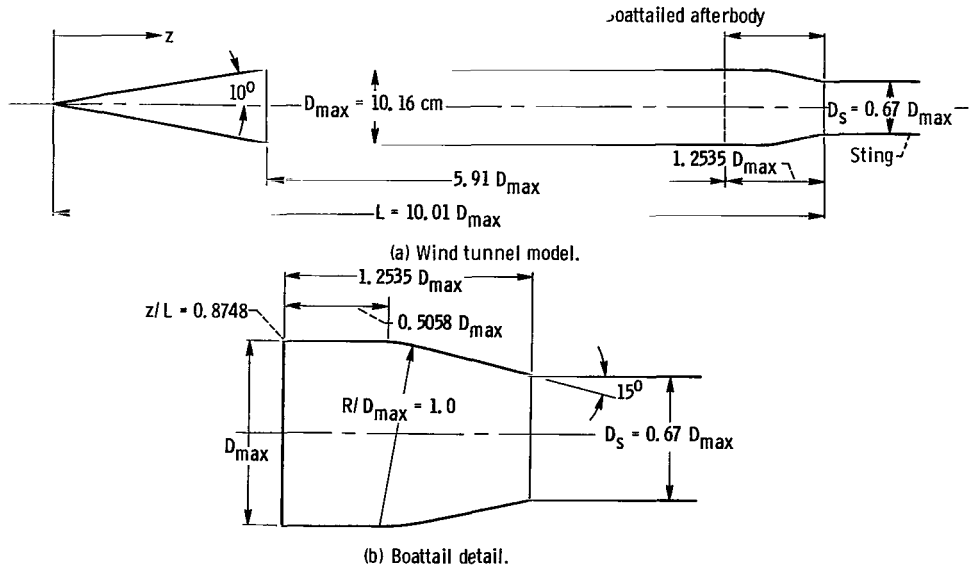
(a) Wind tunnel model.

(b) Boattail detail.

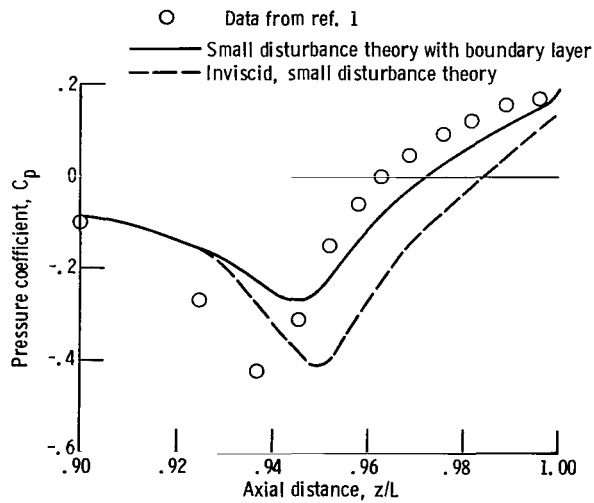Figure 1. – Geometry used for numerical calculations.

Figure 2. – Comparison of pressure distributions calculated from small disturbance theory with data at free-stream Mach 0.80.
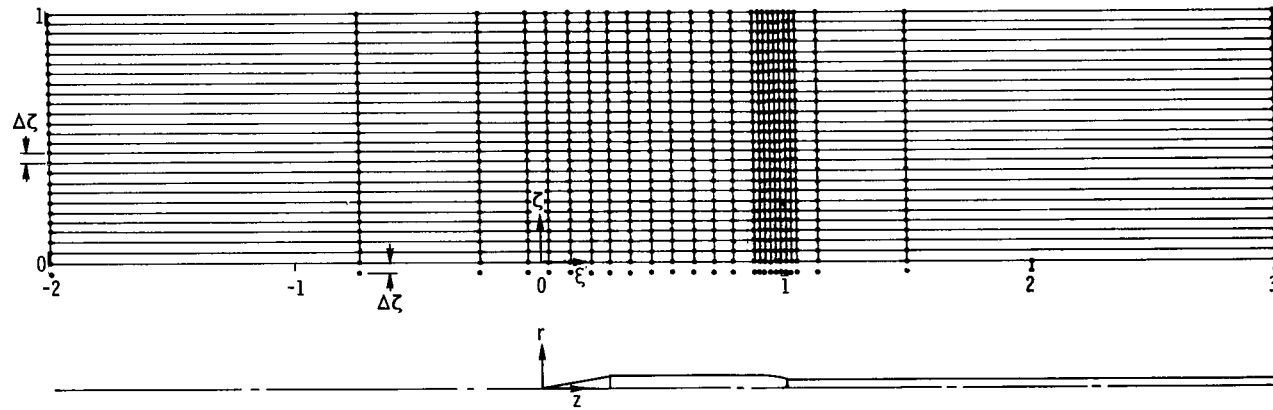
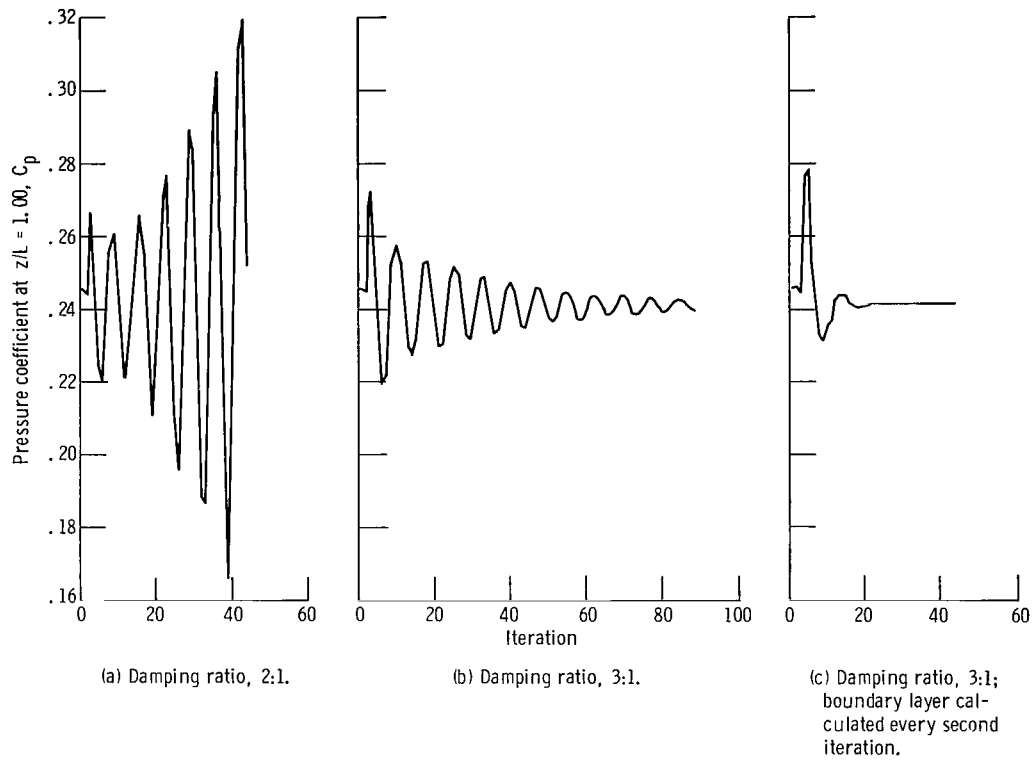Figure 3. – Computational plane with coarse mesh in relation to the actual body.

Figure 4. – Effect of damping displacement thickness on calculated pressure coefficient at end of boattail. Free-stream Mach number, 0.80; 101 x 26 mesh points.
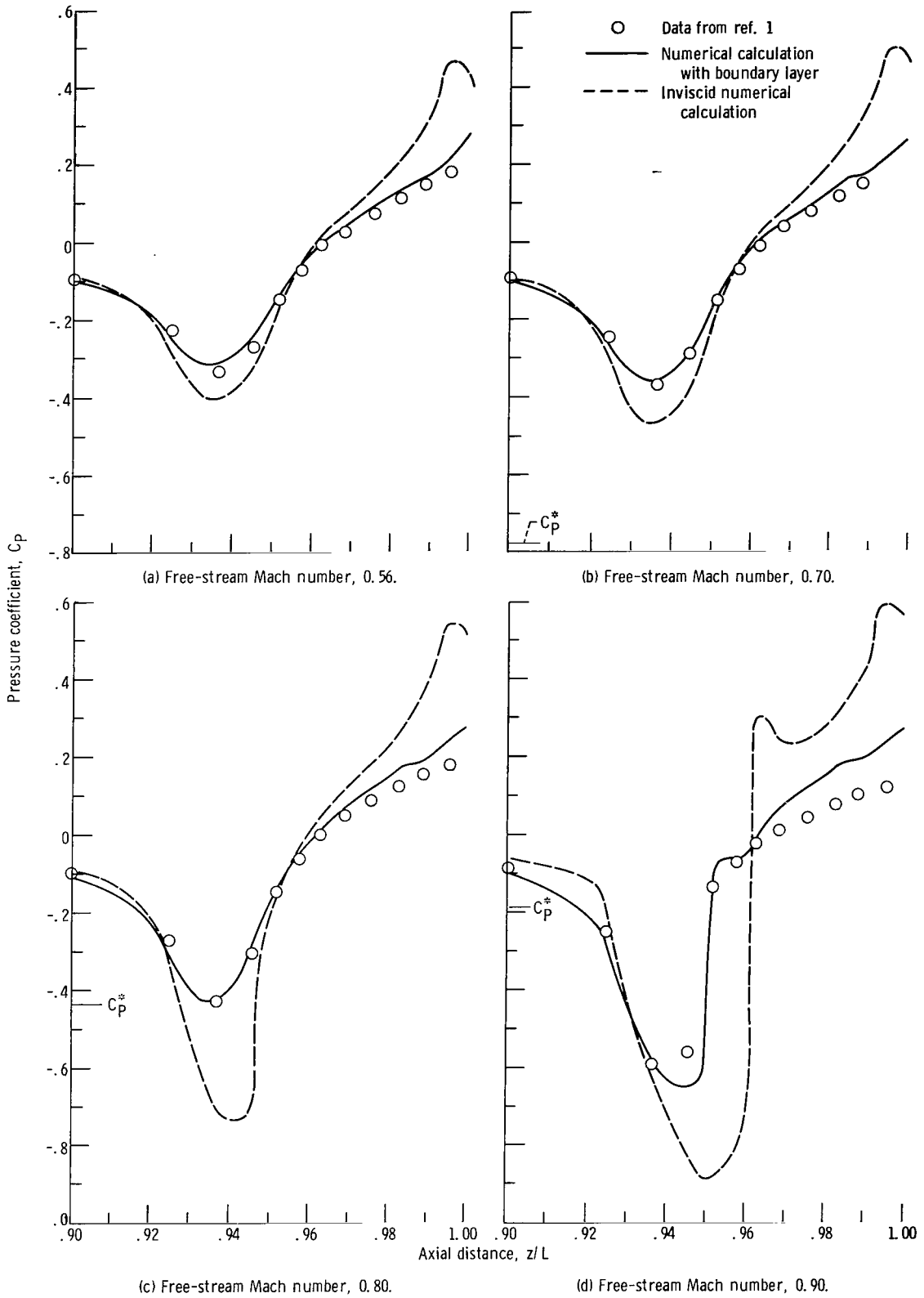
(a) Free-stream Mach number, 0.56.

(b) Free-stream Mach number, 0.70.

(c) Free-stream Mach number, 0.80.

(d) Free-stream Mach number, 0.90.

Figure 5. – Comparison of theoretical and experimental boattail pressure distributions.
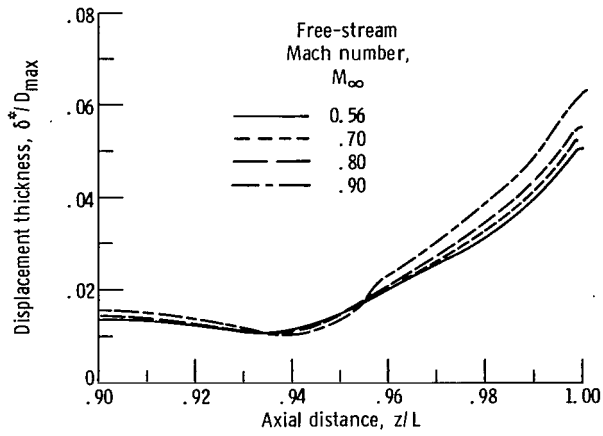
Figure 6. – Calculated displacement thickness along the boattail.
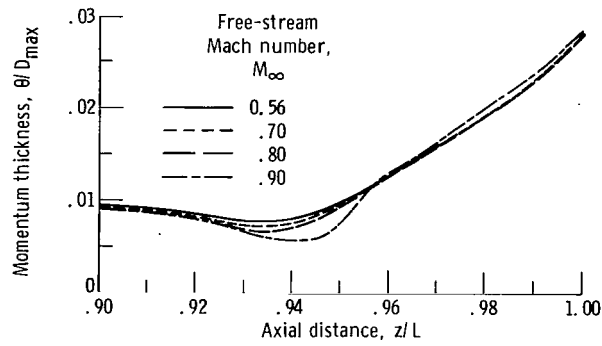
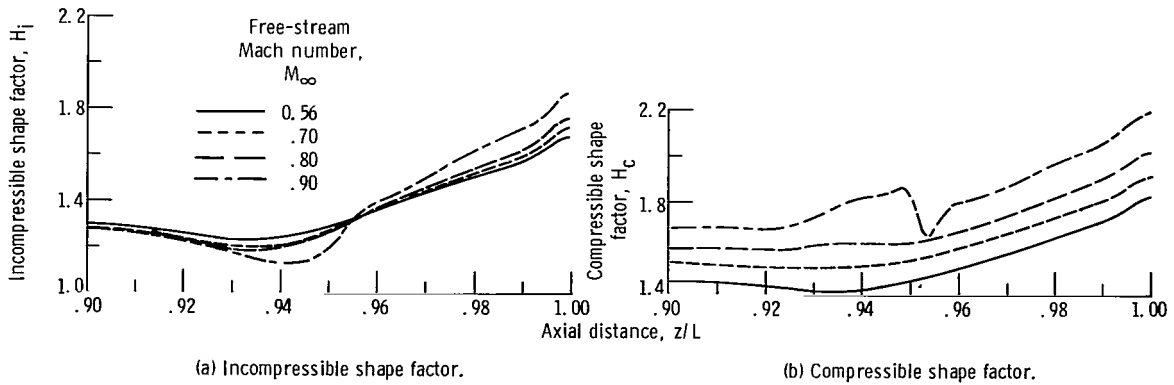Figure 7. – Calculated momentum thickness along the boattail.

(a) Incompressible shape factor.

(b) Compressible shape factor.

Figure 8. – Theoretical shape factors along the boattail.

"The aeronautical and space activities of the United States shall be conducted so as to contribute . . . to the expansion of human knowledge of phenomena in the atmosphere and space. The Administration shall provide for the widest practicable and appropriate dissemination of information concerning its activities and the results thereof."
—NATIONAL AERONAUTICS AND SPACE ACT OF 1958

NASA SCIENTIFIC AND TECHNICAL PUBLICATIONS

TECHNICAL REPORTS: Scientific and technical information considered important, complete, and a lasting contribution to existing knowledge.

TECHNICAL NOTES: Information less broad in scope but nevertheless of importance as a contribution to existing knowledge.

TECHNICAL MEMORANDUMS: Information receiving limited distribution because of preliminary data, security classification, or other reasons. Also includes conference proceedings with either limited or unlimited distribution.

CONTRACTOR REPORTS: Scientific and technical information generated under a NASA contract or grant and considered an important contribution to existing knowledge.

TECHNICAL TRANSLATIONS: Information published in a foreign language considered to merit NASA distribution in English.

SPECIAL PUBLICATIONS: Information derived from or of value to NASA activities. Publications include final reports of major projects, monographs, data compilations, handbooks, sourcebooks, and special bibliographies.

TECHNOLOGY UTILIZATION PUBLICATIONS: Information on technology used by NASA that may be of particular interest in commercial and other non-aerospace applications. Publications include Tech Briefs, Technology Utilization Reports and Technology Surveys.

Details on the availability of these publications may be obtained from:

SCIENTIFIC AND TECHNICAL INFORMATION OFFICE

NATIONAL AERONAUTICS AND SPACE ADMINISTRATION
Washington, D.C. 20546